PCCP

PAPER

View Article Online
View Journal | View Issue

Cite this: *Phys. Chem. Chem. Phys.*, 2014, **16**, 3670

Lithium diffusion in congruent $LiNbO_3$ single crystals at low temperatures probed by neutron reflectometry

E. Hüger,[a] J. Rahn,[a] J. Stahn,[b] T. Geue,[b] P. Heitjans[cd] and H. Schmidt*[ad]

Received 22nd November 2013,
Accepted 23rd December 2013

DOI: 10.1039/c3cp54939a

www.rsc.org/pccp

The self-diffusion of lithium in congruent $LiNbO_3$ single crystals was investigated at low temperatures between 379 and 523 K by neutron reflectometry. From measurements on $^6LiNbO_3$ (amorphous film)/$^{nat}LiNbO_3$ (single crystal) samples, Li self-diffusivities were determined in single crystals down to extremely low values of 1×10^{-25} m^2 s^{-1} on small length scales of 1–10 nm. The measured diffusivities are in excellent agreement with (extrapolated) literature data obtained by experiments based on Secondary Ion Mass Spectrometry and Impedance Spectroscopy. The tracer diffusivities can be described by a single Arrhenius line over ten orders of magnitude with an activation enthalpy of 1.33 eV, which corresponds to the migration energy of a single Li vacancy. A deviation from the Arrhenius behaviour at low temperatures, *e.g.*, due to defect cluster formation is not observed.

1. Introduction

Lithium niobate ($LiNbO_3$) is still one of the most technologically important materials for optical, opto-electronic and piezoelectric applications due to its unique combination of efficient pyroelectric, piezoelectric, electrocaloric, acousto-optical, giant-photovoltaic, ferroelectric, electro-optical, photorefractive and non-linear optical properties.[1–4] These properties are combined with a high available quality, easy fabrication and low cost of single crystals.[1,5] Large ferroelectric, pyroelectric and piezoelectric coefficients are present due to the polar asymmetry of the Li–O cage in the hexagonal crystal structure (space group *R*3*c*).[6–8] Due to its versatile applications in the field of advanced photonics and opto-electronics, $LiNbO_3$ is often termed as the 'silicon of photonics'.[9,10]

$LiNbO_3$ shows a wide solid solution region from 44 mol% to about 50.5 mol% Li_2O.[11] Single crystals produced by the Czochralski method show the congruent composition of about 48.5 mol% Li_2O. However, by using the vapor transport equilibration (VTE) (or other) methods the synthesis of near stoichiometric crystals is also possible.[12] The change of composition from the lithium-poor to the stoichiometric side results in significant changes in the physical properties like the Curie temperature, the ferroelectric coercive field, and photorefractive properties.[13,14] These changes in physical properties are expected to be the result of defect clusters, which are also responsible for the non-stoichiometry. From the models proposed,[15–19,48] the most reliable model consists of a niobium antisite atom which is charge compensated by four lithium vacancies ($Nb_{Li}^{\bullet\bullet\bullet\bullet} + 4V_{Li}'$) as supported by atomistic simulations[18,49] and density calculations.[50]

Many of the above mentioned physical properties can be used in commercial devices only after a low-temperature thermal treatment (<500 K) of $LiNbO_3$ in air or inert gas. The annealing induces the redistribution and diffusion of Li^+ and/or H^+ ions, which improve the technologically useful properties of $LiNbO_3$. Characteristic processes are thermal fixing for optical data storage,[2,3,20–22] purification from unwanted photo-active electrons (optical damage inhibition),[2,3,9,10,23] waveguide fabrication by proton-exchange,[1,2,24–26] and the improvement of ferroelectric domain switching.[3,14,27] In addition, the formation, stability and dissociation of defect clusters are closely related to diffusion properties.[18]

In the literature, several studies on impurity diffusion are available for single crystalline $LiNbO_3$, however, reliable data for Li self-diffusion are very rare (for reviews see ref. 18,28). Li is expected to be the most mobile species compared to Nb and O.[28] Li diffusion experiments are almost exclusively restricted to nuclear magnetic resonance (NMR) studies[28–33] limited to the high-temperature range above 773 K. A diffusion study based on mass tracers and stable isotopes was done at high temperatures above 1000 K.[28,34] We recently presented a study on Li self-diffusion in congruent $LiNbO_3$ single crystals at low temperatures

[a] *Clausthal University of Technology, Institute of Metallurgy, Microkinetics Group, Clausthal-Zellerfeld, Germany. E-mail: harald.schmidt@tu-clausthal.de*
[b] *Laboratory for Neutron Scattering, Paul Scherrer Institut, Villigen PSI, Switzerland*
[c] *Institut für Physikalische Chemie und Elektrochemie, Leibniz Universität Hannover, Germany*
[d] *ZFM – Centre for Solid State Chemistry and New Materials, Leibniz University Hannover, Germany*

down to 423 K which was based on secondary ion mass spectrometry experiments.[35] A dependence of Li diffusion on the crystallographic orientation was not found.[36] In addition, impedance spectroscopy measurements were done on the same type of single crystal,[43] proving that Li is the species that governs conductivity at least down to 473 K. For temperatures below 423 K we are not aware of any Li tracer experiments in the literature. However, a great variety of conductivity measurements done by impedance spectroscopy or by the four-probe dc method are published.[29,37–42] These techniques are not selectively sensitive to Li and often it is unclear which species contributes to conductivity. As well as lithium, hydrogen and electrons are possible charge carriers.

Recently, neutron reflectometry (NR) was applied[44] to bulk materials and this study demonstrated the possibility of determining Li diffusivities in $LiNbO_3$ single crystals. The basic principle of these experiments is the following: first, about 50 nm thick amorphous films of $^6LiNbO_3$ with a high Li diffusivity were ion-beam sputtered onto the (001) faces of $^{nat}LiNbO_3$ single crystals (containing 92.5% ^{7}Li) having a considerably lower diffusivity at the same temperature. Such structures are termed $^6LiNbO_3$ (amorphous film)/$^{nat}LiNbO_3$ (single crystal) isotope heterostructures. Due to the fact that the two Li isotopes have different bound coherent neutron scattering lengths, characteristic interference patterns (fringes) are observed if measured by NR. Diffusion annealing leads to a ^{6}Li/^{7}Li interdiffusion process and to a modification of the NR pattern. This modification is dominated by the slow diffusion of ^{6}Li into the single crystal. The amorphous $^6LiNbO_3$ film itself is a ^{6}Li tracer reservoir, where self-diffusion is tremendously faster than in the $LiNbO_3$ single crystal.[45] ^{7}Li ions that enter the amorphous film from the crystal quickly spread out over the whole film thickness. This process does not significantly alter the NR pattern for small diffusion length up to 10 nm. In contrast, ^{6}Li diffusion in the single crystal is much slower and consequently controls the interdiffusion process. The diffusion of ^{6}Li into the single crystal is modelled by a complementary error-function (see below). From the modification of the neutron reflectivity patterns during annealing, the Li self-diffusivity can be extracted using the fitting procedure Parratt32,[46] which calculates reflectivity using a recursive algorithm.

The diffusion results at 473 and 523 K are in agreement with the Li diffusivities determined by NR on small length scales (1–6 nm) and by SIMS on large length scales (>35 nm).[44] The approach described is applied in the present study to measure the temperature dependence of Li self-diffusivities in lithium niobate below 473 K down to 379 K.

2. Experimental details

For the diffusion experiments, 40–50 nm thick isotope enriched $^6LiNbO_3$ films were deposited by ion-beam sputtering on commercial *c*-axis oriented $^{nat}LiNbO_3$ single crystals (CrysTec, Berlin) with a Li_2O content of 48.5 mol%.[35] Ion beam sputtering was performed using a commercial set-up (IBC 681, Gatan) equipped with two Penning ion sources. Deposition was done at 5 keV and at a current of about 200 μA in argon at an operating pressure of 5×10^{-5} mbar. The base vacuum was better than 5×10^{-7} mbar. As sputter targets, sintered $^6LiNbO_3$ was used. Details of sputter target preparation are given elsewhere.[35] During deposition, the specimen is rotated (30 rotations per minute) and rocked (rock angle: 30° and rock speed: 12° per second) to ensure a uniform coating of the sample.

The isothermal diffusion anneals were carried out in ambient air in the temperature range between 379 and 523 K. A conventional resistance furnace or alternatively, a rapid thermal annealing set-up (AO 500, MBE, Germany) was used for annealing in ambient air. During such anneals the sputtered $LiNbO_3$ layers stay amorphous, as illustrated in ref. 45.

Neutron reflectometry measurements were carried out on two different reflectometers at the Swiss spallation neutron source (SINQ), Villigen, Switzerland. The time-of-flight reflectometer AMOR was used at incoming neutron wavelengths between 0.2 and 0.9 nm. Reflectivity patterns were measured at incident angles between 0.3° and 3°. Further measurements were carried out using the reflectometer MORPHEUS in the $\theta/2\theta$ mode in 0.005° or 0.01° angle steps using a neutron wavelength of 0.5 nm. Profile fitting was done using the Parratt32 code[46] using a resolution of $\Delta q_z/q_z$ = 5%.

3. Results and discussion

Fig. 1 presents characteristic measured neutron reflectivity patterns and the corresponding Parratt32 simulations from which the Li diffusivity in $LiNbO_3$ single crystals is determined. All measured data can be perfectly described by Parratt32 simulations using the model described in detail in ref. 44. The edge of total reflection is seen for all measurements at a critical value of about q_z = 0.014 Å^{-1}. For higher q_z values, the reflectivity decreases. The bare $^{nat}LiNbO_3$ single crystal (Fig. 1a) does not show any superimposed fringes, as can be expected for

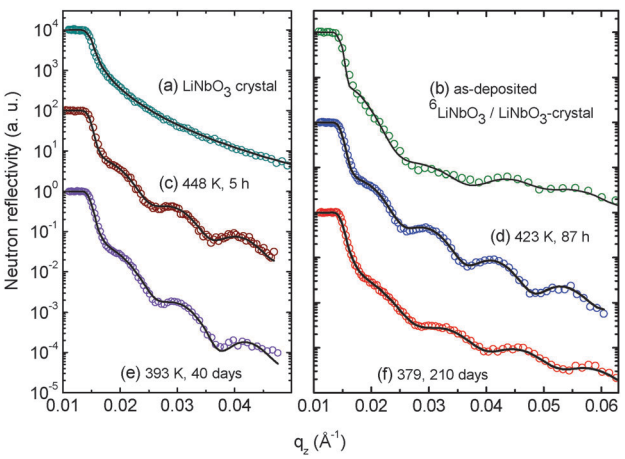

Fig. 1 Measured NR patterns (open symbols) and corresponding Parratt32 simulations (lines) for (a) a pure $^{nat}LiNbO_3$ single crystal and for $^6LiNbO_3$ (amorphous film)/$^{nat}LiNbO_3$ (single crystal) structures in (b) the as-deposited state, and after annealing at (c) 448 K for 5 h, (d) 423 K for 87 h, (e) 393 K for 960 h, and (f) 379 K for 5040 h. For clarity the data are shifted in intensity.

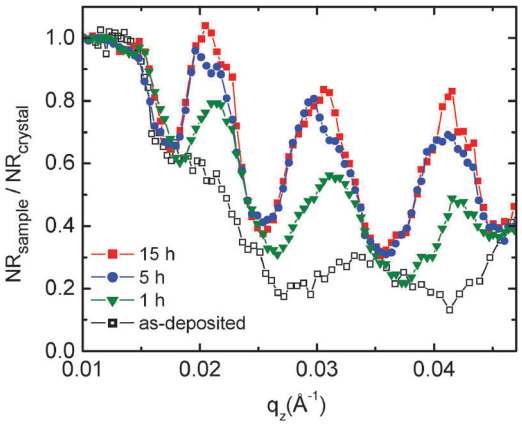

Fig. 2 Normalized reflectivity patterns (NR sample/NR crystal) for a better visualization of the fringe enhancement during diffusion annealing at 448 K for different times.

a bulk single crystal with a smooth surface. Low amplitude fringes appear in Fig. 1b for a single crystal with a sputtered $^{6}LiNbO_3$ layer on top, in the as-deposited state. The reason for these fringes is an interference effect due to a superposition of the neutron beams reflected at the surface and at the $^{6}LiNbO_3$/$^{nat}LiNbO_3$ interface. As is obvious from Fig. 1c–f, diffusion annealing leads to a modification of the neutron reflectivity as a result of ^{6,7}Li isotope interdiffusion. The slight fringes of the as-deposited sample are enhanced. This is especially visible in Fig. 2 where the reflectivity of the $^{6}LiNbO_3$ film/$^{nat}LiNbO_3$ structure (termed the NR sample) is normalized to that of the pure $^{nat}LiNbO_3$ crystal (termed the NR crystal) and plotted on a linear scale. This effect of fringe enhancement is due to the diffusion of ^{6}Li into the $^{nat}LiNbO_3$ single crystal, leading to an increase in scattering length density (SLD) of the crystal close to the isotope interface as shown in Fig. 3.[44] The amorphous $^{6}LiNbO_3$ film is used as a ^{6}Li tracer reservoir, where self-diffusion is tremendously faster than in the $LiNbO_3$ single crystal.[45] ^{7}Li ions that enter the amorphous film from the crystal quickly spread out over the whole film thickness. In contrast, ^{6}Li diffusion in the single crystal is much slower and consequently controls the interdiffusion process. Lithium diffusion data (diffusion length and diffusivity) are extracted from this penetration of ^{6}Li into the $^{nat}LiNbO_3$ single crystal according to the procedure given in ref. 44. Penetration of the ^{6}Li isotope into the single crystal is modelled by a complementary error-function.[44] Consequently, the SLD, ρ, also shows a complementary error-function dependence according to

$$\rho = \rho_{crystal} + (\rho_{interface} - \rho_{crystal}) \cdot \mathrm{erfc}\left(\frac{z}{d\sqrt{2}}\right) \qquad (1)$$

with $\rho_{crystal} = 4.25 \times 10^{-6}$ Å^{-2} and $\rho_{interface} = 4.95 \times 10^{-6}$ Å^{-2}. Here, $\rho_{crystal}$ is the SLD of the bulk $^{nat}LiNbO_3$ single crystal far away from the interface and $\rho_{interface}$ is the SLD at the interface inside the crystal (not in the amorphous $^{6}LiNbO_3$ film) during the diffusion process (see Fig. 3). The latter quantity corresponds to the SLD of a $^{6}LiNbO_3$ single crystal. Further, $d = (2Dt)^{1/2}$ is the diffusion length, D is the diffusivity, and t is the annealing time. The complementary error-function dependence of the SLD according to eqn (1) is implemented in the Parratt32 program in the form of a bar model and detailed fitting of the annealed samples is carried out as described elsewhere.[44] From the fitting results, the diffusion length, d, is extracted which changes significantly with increasing annealing time, while all other parameters are kept constant. The diffusivities are calculated directly from the diffusion length according to $D = d^2/2t$ and are listed in Table 1. The error limits attributed to the diffusion length result from best fitting to the experimental data. The diffusivities are identical within error limits for different anneals at constant temperature. Reliable diffusivities (with error limits below 100%) can be obtained by diffusion experiments where the Li diffusion lengths are between 1.5 and 6.5 nm, in agreement with the theoretical considerations given in ref. 44.

The Li tracer diffusivities obtained by NR are plotted in Fig. 4 as a function of reciprocal temperature. Fig. 5 presents the Li tracer diffusivities obtained by NR in comparison to tracer diffusivities derived from SIMS experiments on the same type of samples[35] and with charge diffusivities as derived from impedance spectroscopy (IS) measurements on the same type

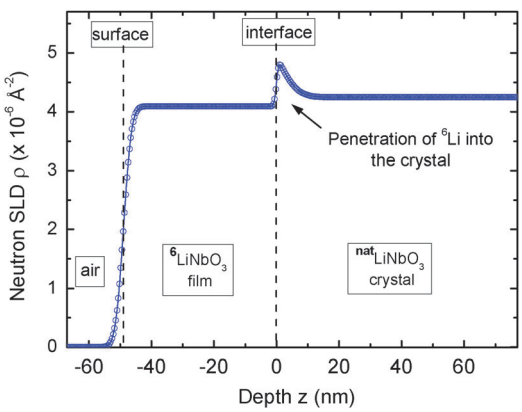

Fig. 3 Neutron scattering length density (SLD) as obtained from the Parratt32 simulations given in Fig. 1d. The space coordinate z is set to zero at the film/crystal interface. For further details it is referred to the text.

Table 1 Annealing temperature, annealing times, diffusion lengths and Li diffusivities as obtained from the NR experiments on congruent $LiNbO_3$ single crystals. The diffusivities given at 473 K and 523 K were already published in ref. 44

Temperature (K)	Annealing time (h)	d (nm)	D (m^2 s^{-1})
523	0.067	4.0 ± 1.0	(3.3 ± 1.7) × 10^{-20}
523	0.250	8.0 ± 3.0	(3.5 ± 2.4) × 10^{-20}
473	0.166	1.5 ± 0.5	(1.8 ± 1.2) × 10^{-21}
473	2	3.5 ± 1.0	(0.9 ± 0.3) × 10^{-21}
473	8	6.0 ± 2.0	(0.6 ± 0.4) × 10^{-21}
448	1	2.0 ± 1.0	(5.6 ± 5.6) × 10^{-22}
448	5	4.0 ± 1.0	(4.4 ± 2.2) × 10^{-22}
423	4	1.5 ± 0.5	(7.8 ± 5.2) × 10^{-23}
423	87	5.0 ± 1.5	(4.0 ± 2.4) × 10^{-23}
423	192	7.0 ± 2.5	(3.6 ± 2.5) × 10^{-23}
393	192	1.5 ± 0.5	(1.6 ± 1.0) × 10^{-24}
393	960	3.5 ± 1.0	(1.8 ± 1.0) × 10^{-24}
379	5040	3.0 ± 1.0	(2.4 ± 1.6) × 10^{-25}

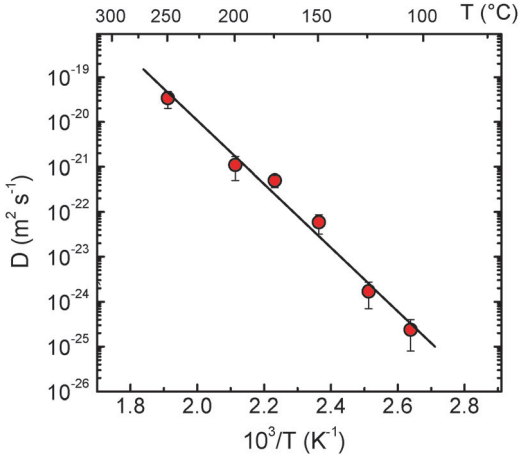

Fig. 4 Diffusivities of Li in $LiNbO_3$ single crystals measured by NR as a function of reciprocal temperature. The straight line corresponds to the Arrhenius fit of the data obtained by NR. The diffusivities at 473 and 523 K were already given in preliminary work, where the realization of the new methodology was demonstrated.[44] The diffusivity given at a certain temperature is an average of the data given in Table 1 for different annealing times.

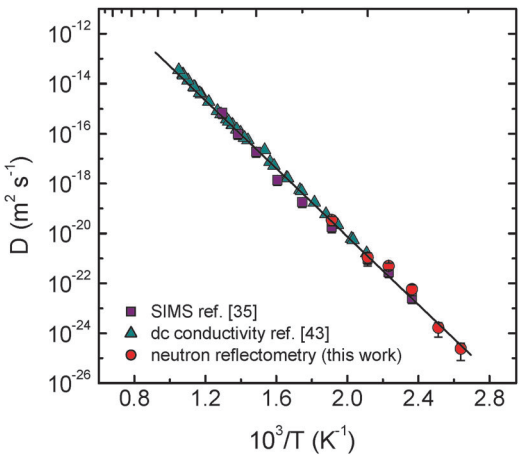

Fig. 5 Diffusivities of Li in $LiNbO_3$ single crystals as a function of reciprocal temperature, in comparison to charge diffusivities as obtained by impedance spectroscopy (ref. 43) and to diffusivities as obtained by SIMS (ref. 35) on the same type of crystal as used in the present study.

of samples.[43] The diffusion data obtained by the different methods (NR, SIMS and IS) are in good agreement with each other. This indicates that the Li^+ is the dominant species that governs conductivity in this type of sample.

The Li diffusivities determined by NR (Fig. 4) follow the Arrhenius law

$$D = D_0 \exp(\Delta H/k_B T) \quad (2)$$

with an activation enthalpy of diffusion $\Delta H = (1.39 \pm 0.07)$ eV and a pre-exponential factor of $D_0 = 1.6 \times 10^{-6}$ m^2 s^{-1} (error: $\ln D_0/\mathrm{m}^2\ \mathrm{s}^{-1} = \pm 2.4$). The tracer diffusivities determined by SIMS and NR jointly follow the Arrhenius law over ten orders of magnitude (Fig. 5). An activation enthalpy of $\Delta H = (1.33 \pm 0.02)$ eV and a pre-exponential factor of $D_0 = 1.6 \times 10^{-7}$ m^2 s^{-1} (error: $\ln D_0/\mathrm{m}^2\ \mathrm{s}^{-1} = \pm 0.7$) can be derived in the temperature range between 379 and 773 K. As pointed out in ref. 35, the activation enthalpy of ΔH = 1.3–1.4 eV can be identified as the activation enthalpy of ionic motion, which is identical to the migration of a single charged Li vacancy in a frozen-in defect structure, even if the temperature is changed.

According to the measurements presented in Fig. 5, no significant effect of the formation of defect clusters on diffusion at low temperatures down to 379 K is observed. Such clusters are expected to be composed of a niobium antisite atom that is surrounded by three lithium vacancies in nearest neighbour positions plus one independent lithium vacancy along the z direction ($Nb_{Li}^{\bullet\bullet\bullet\bullet} + 4V'_{Li}$).[18] At temperatures close to room temperature defect complexes in high concentration are expected to be present in order to explain the variation of physical properties within the solid solution range.[18] Increasing temperature leads to a dissociation of these complexes and the formation of free migrating vacancies. An upper limit for the fraction of these vacancies is provided by the off-stoichiometry of the crystal, which is about 4% at the congruent composition.[19] Lowering the temperature should lead to a decrease of the free vacancy concentration and consequently of the diffusivities by complex formation. Such a lowering of diffusivities is not observed down to 379 K, meaning that the number of complexes is much smaller than the number of free vacancies. For the isostructural compound $LiTaO_3$, a significant recovery of the internal electrical field from a domain reversed state is taking place around 373 K on a time scale of 1–2 h.[47] This means that defect complexes which might be responsible for such a field have to dissociate and vacancies become mobile at the given temperature. The presence of a high number of mobile vacancies can be confirmed in light of the present diffusion experiment on $LiNbO_3$.

4. Conclusion

We carried out diffusivity measurements using neutron reflectometry in order to obtain lithium self-diffusivities in $LiNbO_3$ single crystals at temperatures below 473 K. The methodology allows the temperature range to be extended down to 379 K and the diffusivities to be measured over four orders of magnitude. Together with literature data obtained on the same type of single crystals by various methods (SIMS, impedance spectroscopy) the lithium diffusivity in the temperature range between 379 and 984 K can be described by the Arrhenius law with a single activation energy of 1.3 eV over ten orders of magnitude. A deviation from the Arrhenius behaviour at low temperatures due to defect cluster formation is not observed.

Acknowledgements

This work is based on experiments performed at the Swiss spallation source SINQ, at the instruments AMOR and MORPHEUS, Paul Scherrer Institut, Villigen, Switzerland. Financial

support from the Deutsche Forschungsgemeinschaft (projects: Schm 1569/18 and He 1574/13) in the framework of the Research Unit FOR 1277 ('molife') is gratefully acknowledged. This research has also been supported by the European Commission under the 7th Framework Programme through the 'Research Infrastructures' action of the 'Capacities' Programme, Contract No: CP-CSA_INFRA-2008-1.1.1 Number 226507-NMI3. Thanks are due to B. Ruprecht (Leibniz Universität Hannover) for preparing the $LiNbO_3$ sputter targets.

References

1 Q. Peng and R. E. Cohen, *Phys. Rev. B: Condens. Matter Mater. Phys.*, 2011, **83**, 220103.
2 *Properties of Lithium Niobate, INSPEC Institution of Electrical Engineers*, ed. K. K. Wong, London, 2002.
3 *The Handbook of Photonics*, ed. M. C. Gupta and J. Ballato, CRC Press Taylor & Francis Group, Boca Raton, 2007.
4 T. Volk and M. Wöhleke, *Lithium Niobate*, Springer, Berlin, 2010.
5 F. Lüdtke, K. Buse and B. Sturman, *Phys. Rev. Lett.*, 2012, **109**, 026603.
6 S. C. Abrahams, J. M. Reddy and J. L. Bernstin, *J. Phys. Chem. Solids*, 1966, **27**, 997.
7 H. D. Megaw, *Acta Crystallogr., Sect. A: Cryst. Phys., Diffr., Theor. Gen. Crystallogr.*, 1968, **24**, 583.
8 R. S. Weis and T. K. Gaylord, *Appl. Phys. A: Solids Surf.*, 1985, **37**, 191.
9 B. Sturman, M. Kösters, D. Haertle, C. Becher and K. Buse, *Phys. Rev. B: Condens. Matter Mater. Phys.*, 2009, **80**, 245319.
10 M. Kösters, B. Sturman, P. Werheit, D. Haertle and K. Buse, *Nat. Photonics*, 2009, **3**, 510.
11 P. Lerner, C. Legras and J. Dumas, *J. Cryst. Growth*, 1968, **3**, 231.
12 P. F. Bordui, R. G. Norwood, D. H. Jundt and M. M. Fejer, *J. Appl. Phys.*, 1992, **71**, 875.
13 V. Gopalan, V. Dierolf and D. A. Scrymgeou, *Annu. Rev. Mater. Res.*, 2008, **37**, 449.
14 V. Gopalan, T. E. Mitchell, Y. Furukawa and K. Kitamura, *Appl. Phys. Lett.*, 1998, **72**, 1981.
15 O. F. Schirmer, O. Thiemann and M. Wohlecke, *J. Phys. Chem. Solids*, 1991, **52**, 185.
16 A. Prokhorov and I. Kuzminov, *Physics and Chemistry of Crystalline Lithium Niobate*, Hilger, Bristol, 1990.
17 S. C. Abrahams and P. Marsh, *Acta Crystallogr., Sect. B: Struct. Sci.*, 1986, **42**, 61.
18 H. Xu, D. Lee, S. B. Sinnott, V. Dierolf, V. Gopalan and S. R. Phillpot, *J. Phys.: Condens. Matter*, 2010, **22**, 135002.
19 J. Shi, H. Fritze, G. Borchardt and K.-D. Becker, *Phys. Chem. Chem. Phys.*, 2011, **13**, 6925.
20 D. L. Staebler and J. J. Amodei, *Ferroelectrics*, 1972, **3**, 107.
21 A. Yariv, S. S. Orlov and G. A. Rakuljic, *J. Opt. Soc. Am. B*, 1996, **13**, 2513.
22 K. Buse, S. Breer, K. Peithmann, S. Kapphan, M. Gao and E. Krätzig, *Phys. Rev. B: Condens. Matter Mater. Phys.*, 1996, **56**, 1225.
23 M. Falk, Th. Wolke and K. Buse, *J. Appl. Phys.*, 2007, **102**, 063529.
24 J. Jackel, A. M. Glass and G. E. Peterson, *J. Appl. Phys.*, 1983, **55**, 269.
25 D. P. Birnie, *Ferroelectrics*, 1996, **185**, 29.
26 A. Alcazar, J. Rams, J. M. Cabrera and F. Agullo-Lopez, *J. Appl. Phys.*, 1997, **82**, 4752.
27 H. Steigerwald, M. Lilienblum, Y. J. Ying, R. W. Eason, S. Mailis, B. Sturman, E. Soergel and K. Buse, *Phys. Rev. B: Condens. Matter Mater. Phys.*, 2010, **82**, 214105.
28 D. Birnie III, *J. Mater. Sci.*, 1993, **28**, 302.
29 P. Heitjans, M. Masoud, A. Feldhoff and M. Wilkening, *Faraday Discuss.*, 2007, **134**, 67.
30 M. Wilkening, D. Bork, S. Indris and P. Heitjans, *Phys. Chem. Chem. Phys.*, 2002, **4**, 3246.
31 M. Wilkening and P. Heitjans, *Solid State Ionics*, 2006, **177**, 3031.
32 T. K. Halstead, *J. Chem. Phys.*, 1970, **53**, 3427.
33 D. Bork and P. Heitjans, *J. Phys. Chem. B*, 2001, **105**, 9162.
34 V. B. Ptashnik, T. Y. Dunaeva and I. V. Myasnikov, *Inorg. Mater.*, 1985, **21**, 1814.
35 J. Rahn, E. Hüger, L. Dörrer, B. Ruprecht, P. Heitjans and H. Schmidt, *Phys. Chem. Chem. Phys.*, 2012, **14**, 2427.
36 J. Rahn, L. Dörrer, B. Ruprecht, P. Heitjans and H. Schmidt, *Defect Diffus. Forum*, 2013, **333**, 33.
37 A. Mehta, E. K. Chang and D. M. Smyth, *J. Mater. Res.*, 1991, **6**, 851.
38 S. Klauer, M. Wöhlecke and S. Kapphan, *Phys. Rev. B: Condens. Matter Mater. Phys.*, 1992, **45**, 2786.
39 A. V. Yatsenko, S. V. Yevdokimov, A. S. Pritulenko, D. Y. Sugak and I. M. Solskii, *Phys. Solid State*, 2012, **54**, 2231.
40 W. Bollmann and M. Gernand, *Phys. Status Solidi*, 1972, **9**, 301.
41 K. Brands, M. Falk, D. Haertle, T. Woike and K. Buse, *Appl. Phys. B: Lasers Opt.*, 2008, **91**, 279.
42 A. Weidenfelder, J. Shi, P. Fielitz, G. Borchardt, K. D. Becker and H. Fritze, *Solid State Ionics*, 2012, **225**, 26.
43 B. Ruprecht, J. Rahn, H. Schmidt and P. Heitjans, *Z. Phys. Chem.*, 2012, **226**, 431.
44 E. Hüger, J. Rahn, J. Stahn, T. Geue and H. Schmidt, *Phys. Rev. B: Condens. Matter Mater. Phys.*, 2012, **85**, 214102.
45 J. Rahn, E. Hüger, L. Dörrer, B. Ruprecht, P. Heitjans and H. Schmidt, *Z. Phys. Chem.*, 2012, **226**, 439.
46 C. Braun, Parratt32 or the reflectometry tool, HMI, Berlin, 1997–1999, http://www.helmholtz-berlin.de.
47 S. Kim, V. Gopalan, K. Kitamura and Y. Furukawa, *J. Appl. Phys.*, 2001, **90**, 2949.
48 H. J. Donnerberg, S. M. Tomlinson and C. R. A. Catlow, *J. Phys. Chem. Solids*, 1991, **52**, 201.
49 R. M. Araujo, K. Lengyel, R. A. Jackson, L. Kovacs and M. E. G. Valerio, *J. Phys.: Condens. Matter*, 2007, **19**, 046211.
50 L. Kovacs and K. Polgar, *Cryst. Res. Technol.*, 1986, **21**, K101.